

Journal Pre-proof



Metabolic regulation of macrophages by SIRT1 determines activation during cholestatic liver disease in mice

Anna Isaacs-Ten, Mar Moreno-Gonzalez, Caitlin Bone, Andre Martens, Federico Bernuzzi, Tobias Ludwig, Charlotte Hellmich, Karsten Hiller, Stuart A. Rushworth, Naiara Beraza

PII: S2352-345X(21)00260-5
DOI: <https://doi.org/10.1016/j.jcmgh.2021.12.010>
Reference: JCMGH 937

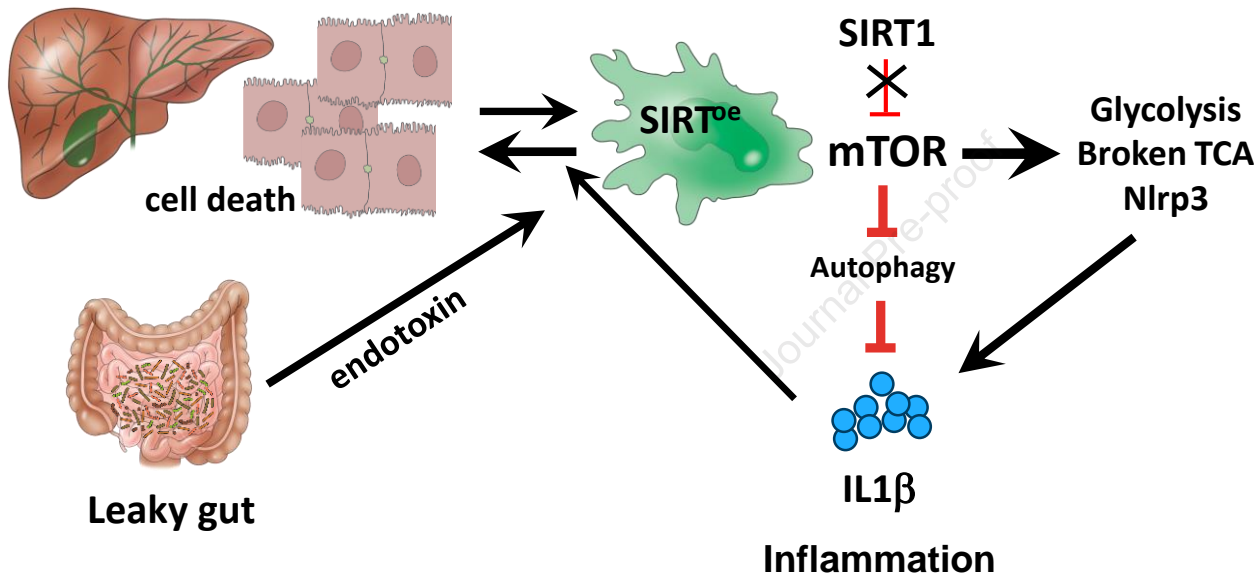
To appear in: *Cellular and Molecular Gastroenterology and Hepatology*
Accepted Date: 13 December 2021

Please cite this article as: Isaacs-Ten A, Moreno-Gonzalez M, Bone C, Martens A, Bernuzzi F, Ludwig T, Hellmich C, Hiller K, Rushworth SA, Beraza N, Metabolic regulation of macrophages by SIRT1 determines activation during cholestatic liver disease in mice, *Cellular and Molecular Gastroenterology and Hepatology* (2022), doi: <https://doi.org/10.1016/j.jcmgh.2021.12.010>.

This is a PDF file of an article that has undergone enhancements after acceptance, such as the addition of a cover page and metadata, and formatting for readability, but it is not yet the definitive version of record. This version will undergo additional copyediting, typesetting and review before it is published in its final form, but we are providing this version to give early visibility of the article. Please note that, during the production process, errors may be discovered which could affect the content, and all legal disclaimers that apply to the journal pertain.

© 2021 The Authors. Published by Elsevier Inc. on behalf of the AGA Institute.

Cholestasis



Metabolic regulation of macrophages by SIRT1 determines activation during cholestatic liver disease in mice

Short title: SIRT1 controls macrophage activation during cholestasis

Anna Isaacs-Ten^{*1}, Mar Moreno-Gonzalez^{*1}, Caitlin Bone^{*1}, Andre Martens², Federico Bernuzzi³, Tobias Ludwig², Charlotte Hellmich^{4,5}, Karsten Hiller^{2,6}, Stuart A. Rushworth^{4,7}, Naiara Beraza^{1,3,7}

* AIT, MMG and CB contributed equally to this work

¹Gut Microbes and Health Institute Strategic Programme, Quadram Institute Bioscience, Norwich Research Park, Norwich, UK, ²Department of Bioinformatics and Biochemistry, Braunschweig Integrated Center of Systems Biology (BRICS), Braunschweig, Germany.

³Food Innovation and Health Institute Strategic Programme, Quadram Institute Bioscience, Norwich Research Park, Norwich, UK, ⁴Faculty of Medicine, University of East Anglia, Norwich, Norfolk, UK ⁵Department of Haematology, Norfolk and Norwich University Hospitals NHS Trust, Colney Lane, NR4 7UY Norwich, UK ⁶Computational Biology of Infection Research, Helmholtz Centre for Infection Research, Braunschweig, Germany.

⁷To whom correspondence should be addressed.

Corresponding Authors:

Naiara Beraza, PhD

Gut Microbes and Health institute strategic programme; Food Innovation and Health institute strategic programme, Quadram Institute, Norwich Research Park, Norwich, NR4 7UQ, United Kingdom.

e-mail: naiara.beraza@quadram.ac.uk

Tel. 0044(0)1603251413

Stuart Rushworth, PhD

Norwich Medical School, University of East Anglia, Norwich Research Park, Norwich, NR4 7UQ, United Kingdom.

e-mail: S.Rushworth@uea.ac.uk

Word count: 4804

Conflict of Interest Statement: All authors declare that they have no competing financial interests with respect to this manuscript.

Acknowledgements:

The authors gratefully acknowledge the support of the Biotechnology and Biological Sciences Research Council (BBSRC); this research was funded by the BBSRC Institute Strategic Programme Gut Health and Food Safety BB/J004529/1, the BBSRC Gut Microbes and Health BBS/E/F/00044509 (to NB), the BBSRC Institute Strategic Programme Gut Microbes and Health BB/R012490/1 and its constituent project BBS/E/F/000PR10355, and the BBSRC Core Capability Grant BB/CCG1860/1 as well as the BBSRC Institute Strategic Programme Food Innovation and Health BB/R012512/1 and its constituent project BBS/E/F/000PR10347. MMG and CB were supported by the BBSRC Institute Strategic Programme Gut Microbes and Health BB/R012490/1 and its constituent project BBS/E/F/000PR10355.

AIT and FB received also support from the BBSRC Doctoral Training Partnership programme. The Medical Research Council MR/T02934X/1 (SAR) and the Wellcome Trust Clinical Research Fellowship (CH). Part of this work received funding from the Deutsche Forschungsgemeinschaft (DFG, German Research Foundation) project HI1400/3-1 (to KH).

We thank Prof. Manuel Serrano for kindly providing us with the SIRT1-overexpressing mice.

Authors' contributions:

Anna Isaacs-Ten: Investigation, Formal analysis, Writing methods.

Mar Moreno-Gonzalez: Investigation, Formal analysis

Caitlin Bone: Investigation

Andre Martens: Investigation, Formal analysis, Visualization, Writing, Resources

Federico Bernuzzi: Investigation

Tobias Ludwig: Investigation, Resources

Charlotte Hellmich: Investigation

Karsten Hiller: Investigation, Formal analysis, Visualization, Writing, Supervision, Resources,
Funding acquisition, validation

Stuart A. Rushworth: Investigation, Formal analysis, Writing, Supervision, Resources,
Funding acquisition

Naiara Beraza: Investigation, Formal analysis, Visualization, Writing, Supervision, Resources,
Funding acquisition, validation, Project administration, Conceptualization

Synopsis

Here, we describe that the SIRT1/mTOR axis regulates metabolic rewiring, inflammasome activation and autophagy in macrophages, where SIRT1 overexpression actively contributes to aggravate cholestatic liver disease progression in mice.

Journal Pre-proof

Background & Aims: Inflammation is the hallmark of chronic liver disease. Metabolism is a key determinant to regulate the activation of immune cells. Here we define the role of Sirtuin1 (SIRT1), a main metabolic regulator, in controlling the activation of macrophages during cholestatic liver disease and in response to endotoxin.

Methods: We have used mice overexpressing SIRT1 which we treated with intraperitoneal LPS or induced cholestasis by the ligation of the bile duct (BDL). Bone Marrow Derived Macrophages were used for mechanistic *in vitro* studies. Finally, PEPC-Boy mice were used for adoptive transfer experiments to elucidate the impact of SIRT1 overexpressing macrophages in contributing to cholestatic liver disease.

Results: We found that SIRT1 overexpression promotes increased liver inflammation and liver injury after LPS/GaIN and BDL; this was associated with an increased activation of the inflammasome in macrophages. Mechanistically, SIRT1 overexpression associated with the activation of the mTOR pathway that led to increased activation of macrophages, which showed metabolic rewiring with increased glycolysis and broken TCA cycle in response to endotoxin *in vitro*. Activation of the SIRT1/mTOR axis in macrophages associated with the activation of the inflammasome and the attenuation of autophagy. Ultimately, in an *in vivo* model of cholestatic disease, the transplantation of SIRT1 overexpressing myeloid cells contributed to liver injury and fibrosis.

Conclusions: Our study provides novel mechanistic insights into the regulation of macrophages during cholestatic disease and the response to endotoxin, where the SIRT1/mTOR crosstalk regulates macrophage activation controlling the inflammasome, autophagy and metabolic rewiring.

Keywords: SIRT1, metabolism, macrophages, inflammasome, cholestasis

During chronic liver disease, the accumulation of dying cells in the liver together with the translocation of bacteria (products) from a leaky gut contribute to disease progression by sustaining inflammation [1-3]. Macrophages are the first line of defence to respond to bacteria and to remove cellular debris and thus play an essential role during chronic disease, where proinflammatory macrophages infiltrate the liver and contribute to disease progression and fibrosis [4-6]. The mechanisms controlling macrophage function are complex and it is now apparent that metabolic rewiring, the regulation of the inflammasome and autophagy are essential to regulate macrophage activation [7-11].

In the last decade, the development of new metabolomic techniques has contributed to establishing the role of metabolism in regulating macrophage function showing increased glycolysis and a rewired TCA cycle during activation [7]. The influence of metabolic reprogramming in controlling macrophage activation expands to the regulation of the inflammasome, as glycolysis regulates Nlrp3-dependent inflammasome activation [8] while succinate accumulating from a broken TCA promotes IL1 β expression [9]. The inflammasome, a multiprotein complex assembled in the cytosol after pathogen recognition receptors (PRRs) engage with bacteria (products) [12] is activated during human [2] and murine cholestatic disease, where it mediates the progression of the disease as we and others have described [1, 2, 13-15].

Recent evidence supports the role of key metabolic regulators, including Mammalian Target of Rapamycin (mTOR), in modulating inflammation [16, 17]. mTOR is a protein kinase formed by two subunits with differential functions: mTORC1 and mTORC2 [18, 19]. mTORC1 regulates the activation of the Nlrp3-inflammasome in macrophages by promoting glycolysis [8]. Additionally, mTORC1 inhibits autophagy [11] and thus controls the activation of the inflammasome [20].

Sirtuin 1 (SIRT1) is a multifaceted histone deacetylase that controls cell energy and metabolism [21]. SIRT1 was initially described to mediate the benefits of calorie restriction in prolonging the lifespan of lower organisms [22]. Those findings were further challenged and proved to be tissue-specific [23], underlining the complexity of the role of SIRT1 in

controlling mammalian cell function. We and others have demonstrated that SIRT1 is highly expressed in human liver tumours [24-26]. More recently, we described that SIRT1 is upregulated in the liver of patients with chronic cholestatic disease and in cholestatic mice, where we showed that the overexpression of SIRT1 contributed to liver injury and fibrosis [27]. In that context, we found increased inflammation in SIRT1 overexpressing mice, which contrasts with its previously described anti-inflammatory effects [28-32].

Here, we further define the role of SIRT1 in regulating macrophage activation during cholestasis and in response to endotoxin. Our results provide mechanistic evidence of the role of SIRT1 in regulating macrophage activation by modulating cell metabolism, the inflammasome and autophagy. Ultimately, we demonstrate that the overexpression of SIRT1 in macrophages contributes to the aggravation of cholestasis-mediated liver injury by promoting inflammation and fibrosis.

RESULTS

The overexpression of SIRT1 promotes increased inflammasome activation in the liver during cholestasis

We previously described that SIRT1 expression was increased in the livers from Primary Sclerosing cholangitis (PSC) and Primary Biliary cholangitis (PBC) patients as well as in mice following bile duct ligation (BDL) and that the overexpression of SIRT1 contributed to cholestatic disease progression in SIRT1-overexpressing mice (SIRT^{oe}) after BDL [27].

Here, we show that, in addition to the up regulation in hepatocytes we previously described [27], SIRT1 expression is also increased in macrophages (CD11b⁺/F4/80⁺) isolated from livers of WT mice at 7 days after BDL (Fig 1A, B).

Next, we found that SIRT^{oe} mice (Fig 1C) had increased inflammation, characterised by the higher presence of F4/80 (Fig 1D) and CD11b (Fig 1E) positive cells in the liver compared to WT animals at 7 days after BDL. FACS analysis confirmed the increased infiltration of macrophages (CD11b⁺/F4/80⁺/Ly6C⁺) in livers from SIRT^{oe} compared to WT mice at 7 days after BDL (Fig 1F, G).

Macrophages sense dying cells and bacteria via PRRs (e.g. TLR) that activate the Nlrp3-inflammasome to promote the proteolytic cleavage of Pro-Caspase1 into Caspase1 that further cleaves pro-IL β into IL1 β ; its mature form [12]. During cholestasis, the activation of the Nlrp3-inflammasome in macrophages plays a key role in contributing to disease progression [2, 13, 14, 33]. In line with the more severe phenotype, we observed in SIRT^{oe} mice after BDL, we found increased gene expression of TLR-2, TLR-4 and TLR-9, Nlrp3 and Caspase-1 genes in SIRT^{oe} mice compared to WT 7 days after BDL (Fig 2A). These results were confirmed by western blot analysis showing an apparent increase in TLR2, and Nlrp3, as well as higher protein expression of cleaved Caspase-1 and cleaved IL1 β in livers from SIRT^{oe} mice after BDL compared to WT, while mild regulation of TLR4 was observed (Fig 2B).

Previous studies have shown that the activation of the inflammasome during cholestasis is restricted to non-parenchymal cells and specifically to macrophages in PSC patients and in mice after BDL [2, 13, 14, 33]. Our results obtained from immunofluorescence (IF) staining of liver sections confirmed that Nlrp3 co-localised with CD11b (Fig 2C), and Ly6C (Fig 2D) positive cells in livers from WT and SIRT^{oe} mice 7 days after BDL. In addition, IF analyses confirmed the co-localisation of IL1 β in Ly6C positive cells in livers at 7 days after BDL (Fig 2E). Ultimately, we isolated CD11b⁺/F4/80⁺ macrophages from mouse livers at 7 days after BDL and found that SIRT^{oe}-isolated cells had increased IL1 β protein expression compared to WTs (Fig 2F). Overall, these results support that the inflammasome activation we observed in total liver samples was originated mainly in macrophages as previously described [2, 13, 14, 33].

Interestingly, the proinflammatory phenotype observed was accompanied by an increase in IL-10 and IL-4 expression in livers from SIRT^{oe} mice after BDL compared to WTs (Fig 2G, H), supporting that a pro- and anti-inflammatory phenotype can coexist in macrophages beyond the classical M1/M2 polarisation in the liver during disease [34-36].

Chronic liver disease, including cholestasis, associates with the disruption of the intestinal barrier function characterised by increased intestinal permeability ('leaky gut') ([1, 3, 37, 38]). This allows the translocation of bacteria (and their products, i.e. endotoxins) into the liver via the systemic circulation [39], aggravating inflammation and thus disease progression [1]. The increased inflammation and activation of the inflammasome we observed in SIRT^{oe} mice could associate with the higher presence of bacteria (products) in the liver due to increased intestinal permeability [1, 38]. In accordance, we detected higher FITC-labelled dextran in circulation in SIRT^{oe} mice at 3 days after BDL compared to WTs denoting increased intestinal leakage that could contribute to the increased liver inflammation observed (Fig 2I).

Overall, we here describe that during cholestasis, SIRT1 is upregulated and its overexpression associates with increased liver inflammation and inflammasome activation in macrophages after BDL.

Endotoxin promotes increased liver injury and inflammation in the liver of SIRT1 overexpressing mice

Following the leaky gut hypothesis [1, 3, 37, 38], the higher inflammation/inflammasome activity found in SIRT^{oe} mice after BDL could result from the increased liver injury, the higher translocation of bacterial products from a more permeable gut and/or the intrinsic overactivation of macrophages.

To determine this, we treated WT and SIRT^{oe} mice with LPS/GaIN. As shown in Fig 3A, SIRT^{oe} mice showed signs of increased liver injury as evidenced by higher ALT and AST levels 6 hours after LPS/GaIN. Histopathological analysis on liver sections confirmed the more profound parenchymal damage in SIRT^{oe} mice 6 hours after LPS/GaIN compared to WT animals (Fig 3B). Further analysis of PARP protein cleavage supported the increased liver apoptosis in SIRT^{oe} mice after LPS/GaIN (Fig. 3C).

Next, we determined the impact of LPS/GaIN treatment on the inflammatory response in the liver. Our results show that SIRT^{oe} mice have increased presence of F4/80 (Fig 3D) and CD11b (Fig 3E) positive cells in the liver at 6h after LPS/GaIN treatment compared to WT mice.

In line with this, LPS/GaIN treatment resulted in increased TLR4, Nlrp3 and Caspase1 gene expression in SIRT^{oe} mice compared to WT animals (Fig 4A). Our results showing higher cleaved IL1 β protein (Fig 4B) support the stronger activation of the inflammasome in livers from mice overexpressing SIRT1 after LPS/GaIN compared to WTs. IF co-stainings of Nlrp3 and CD11b (Fig 4C) as well as co-stainings of Ly6C and Nlrp3 (Fig 4D) and Ly6C and IL1 β (Fig 4E) confirmed the localisation of the inflammasome in

macrophages in mouse livers after LPS/GaIN treatment, which was higher in SIRT^{oe} mice compared to WTs.

Further *in vitro* analyses comparing the expression levels of inflammasome components in hepatocytes and macrophages showed marginal response to LPS in hepatocytes compared to BMDM (Fig 4F-H). This supports macrophages as the main source of inflammasome-activation we observed in response to LPS *in vivo*.

The increased susceptibility to LPS-induced liver injury and inflammation in SIRT^{oe} mice was confirmed in mice treated with LPS alone for up to 14h, where we found increased ALT/AST levels (Fig 5A), elevated IL1 β gene expression (Fig 5B) and protein cleavage (Fig 5C) when compared to WT mice.

Interestingly, the analysis of isolated primary hepatocytes exposed to endotoxin *in vitro*, showed that LPS had a comparable mild impact on hepatocyte cell death in SIRT^{oe} and WT cells (Fig 5D). This result suggests that the exacerbated liver injury observed in SIRT^{oe} mice *in vivo* may result from the increased inflammatory response mediated by activated macrophages rather than a direct effect of LPS on hepatocyte cell death.

SIRT1 overexpression concurs with mTORC1 activation and contributes to the activation of macrophages by activating the inflammasome and attenuating autophagy

To confirm the role of SIRT1 in controlling macrophage activation and the underlying mechanisms mediating this effect we isolated and differentiated bone marrow derived macrophages (BMDM) from WT and SIRT^{oe} mice. Stimulation with LPS increased IL1 β expression in SIRT^{oe} BMDM compared to WT cells (Fig 6A), which challenges the previously described anti-inflammatory role of SIRT1 based on the attenuation of NF- κ B activity [31]. To determine this, we performed immunocytochemistry analysis on LPS-BMDM that evidenced a delayed nuclear translocation of p65 in SIRT^{oe} BMDM after LPS compared to WT cells rather than a complete inhibition (Fig 6B).

The activation of the inflammasome can be regulated by different signalling pathways, including mTORC1 [8]. mTORC1 activation leads to the downstream activation of S6 Kinase 1 that phosphorylates the ribosomal S6 protein [18, 19]. Our results showed that pS6 was phosphorylated earlier in SIRT^{oe} BMDM than in WT cells after LPS treatment, indicating increased mTORC1 activation in SIRT^{oe} cells (Fig 7A). Furthermore, the inhibition of mTORC1 with Rapamycin showed a more profound attenuation of IL1 β production in SIRT^{oe} cells compared to WT cells after LPS, supporting the higher dependency of SIRT1 overexpressing cells on the mTOR pathway to secrete IL1 β in response to LPS compared to WT BMDM (Fig 7B).

The proinflammatory function of mTORC1 is also supported by its capacity to inhibit autophagy via the phosphorylation of ULK in serine 757 [11]. In turn, autophagy negatively regulates inflammation via inhibiting the inflammasome activation [40]. Accordingly, we found increased presence of pULK757 in SIRT^{oe} BMDM than in WT cells after LPS treatment, confirming increased activation of the mTOR pathway in SIRT^{oe} BMDM (Fig 7C). p62/SQSTM1 (herein p62) is an adaptor protein that contributes to the mTORC1-mediated regulation of autophagy. Additionally, p62 is a substrate of autophagy that accumulates when autophagy is impaired [41]. Our results show strong accumulation of p62 in SIRT^{oe} BMDM compared to WT cells after LPS treatment, pointing to the attenuation of autophagy in the SIRT1 overexpressing cells (Fig 7C).

During autophagy, cytosolic material is engulfed in the autophagosome; a double-membrane structure coated with lipidated LC3II that directs it to the lysosome for fusion into an autolysosome [11]. Our results show that LPS induced accumulation of the lipidated LC3II subunit in WT BMDM after inhibition of the autophagy flux with ammonium chloride/leupeptin pre-treatment, while SIRT^{oe} cells had higher expression of LC3I and lower LC3II (Fig 7D). Immunocytochemistry analysis and further quantification confirmed the increased presence of LC3-puncta, consistent with phagosome formation, in WT BMDM after LPS treatment (Fig 7E, F), supporting the attenuation of autophagy in SIRT^{oe} BMDM.

Overall, our *in vitro* results indicate that the overexpression of SIRT1 associates with the concomitant activation of mTORC1 that leads to the activation of the inflammasome and the attenuation of autophagy, overall promoting the proinflammatory activity of macrophages.

Overexpression of SIRT1 promotes metabolic rewiring of TCA cycle and increased glycolysis in macrophages

Metabolic reprogramming is key to control the inflammatory response in macrophages. A hallmark of this reprogramming is the rewiring of the TCA cycle; the so-called 'broken' TCA cycle, which enables the accumulation of metabolic intermediates; citrate, succinate and fumarate [7, 42]. It is now obvious that these metabolites regulate the inflammatory response (i.e. IL1 β). Thus, citrate is key for the synthesis of itaconate, a hallmark of macrophage activation that contributes to accumulation of intracellular succinate [43-45], essential to sustain inflammation by promoting increased IL1 β levels via glycolysis in macrophages [9].

To elucidate the effect of SIRT^{oe} in LPS-activated macrophages, we first measured intracellular levels of TCA cycle related metabolites. As expected, we found increased levels of citrate, itaconate, succinate and malate after LPS activation (Fig 8A). Interestingly, the levels of itaconate and malate were already increased in resting macrophages overexpressing SIRT1 (Fig 8A). This effect was more pronounced in LPS-macrophages; especially the significantly increased levels of itaconate and succinate indicating a further activation of SIRT^{oe} macrophages (Fig 8A).

To further investigate TCA cycle metabolism, we performed stable isotope labelling experiments and incubated SIRT^{oe} and WT BMDMs in the presence of a [U-¹³C]-glucose tracer. These experiments grant insight into intracellular glucose derived fluxes, as the labelled glucose is metabolized within the cells and the carbon isotopes are incorporated in

downstream metabolites, resulting in specific enrichment patterns (Fig 8B for atom transitions) [46, 47].

LPS stimulation resulted in an increased flux of glycolytic carbon through PDH, displayed by an increased fraction of M2 citrate, M1 itaconate, M2 succinate and M2 malate isotopologues. This flux was even further increased in SIRT^{oe} BMDMs as compared to WT cells. The increased fraction of M1 itaconate isotopologues indicated an even higher synthesis rate of itaconate in SIRT^{oe} BMDMs which agrees with the increased itaconate concentrations. (Fig 8C).

In addition, we analysed the TCA cycling flux by calculating the ratio of M4 to M2 isotopologues of TCA metabolites. We observed a significant reduction of TCA cycle activity under LPS stimulation, which was further attenuated in SIRT^{oe} BMDMs, although the glycolytic flux into the TCA was increased (Fig 8D). One reason for this reduction could be the depletion of NAD⁺ pools by SIRT1 activity. All the above-described findings indicate the rewiring of the TCA cycle, which is specific for LPS activation (8). As the effects are consistently stronger in SIRT^{oe} BMDMs, SIRT1 therefore seems to increase the proinflammatory response in macrophages.

Overexpression of SIRT1 in myeloid cells actively contributes to liver injury and fibrosis during cholestasis

During chronic liver disease, infiltrating, proinflammatory macrophages dominate the liver macrophage pool and actively contribute to disease progression and fibrosis [4-6]. Thus, while the inhibition of infiltrating macrophages attenuates the fibrotic response [48], the transfer of anti-inflammatory macrophages effectively reduces liver fibrosis in mice [49].

We found that macrophages overexpressing SIRT1 were hyperactivated, which could contribute to the exacerbated liver parenchymal injury observed in cholestatic SIRT^{oe} mice [27]. To determine the impact of SIRT1 overexpression in myeloid cells (Fig 9A), and not hepatocytes or other non-inflammatory cells, during the liver response to cholestatic injury *in vivo*, we adoptively transferred LK (lineage negative cKIT positive) cells from WT or

SIRT^{oe} mice (expressing CD45.2) into PEPCBoy recipient mice (expressing CD45.1; herein PEPC) (Fig 9B). The differential expression of CD45 in the donor vs recipient mice allowed us to confirm the engraftment of donor cells in the PEPC recipient mice (Fig 9B). Four weeks after engraftment, we performed BDL in both PEPC+WT and PEPC+SIRT^{oe} mice and analysed the liver parenchyma after 7 days. Our results showed that PEPC+SIRT^{oe} mice had increased liver injury (Fig 9C), with livers showing wide areas of necrosis (Fig 9D). This damaging phenotype associated with higher activation of the inflammasome as evidenced by increased cleaved Caspase1 (Fig 9E) and cleaved IL1 β (Fig 9F) compared to PEPC+WT mice after BDL. PEPC mice receiving SIRT^{oe} cells showed also increased ductular reaction evidenced by CK19 immunostaining (Fig 9G). Ultimately, we found increased fibrosis in PEPC+SIRT^{oe} mice compared to mice receiving PEPC+WT mice at 7 days after BDL, as evidenced by Sirius Red staining (Fig 9H) and α -SMA immunohistochemistry on liver sections and further quantification (Fig 9I).

Overall, our results show that SIRT1 overexpression in myeloid cells contributes to cholestatic disease progression by aggravating liver injury and fibrosis.

DISCUSSION

In this study, we demonstrate that SIRT1 regulates liver inflammation by controlling the activation of macrophages in response to endotoxin and during cholestatic liver disease. Mechanistically, we show that the overexpression of SIRT1 associates with mTOR activation, metabolic rewiring, the activation of the inflammasome and attenuation of autophagy in macrophages. Ultimately, we demonstrate that the overexpression of SIRT1 in myeloid cells contributes to cholestatic disease progression, promoting liver damage and fibrosis.

Chronic liver disease progression is driven by hepatocellular cell death, triggering inflammation, fibrosis and end-stage liver disease [50]. In addition, liver disease associates with increased intestinal permeability that allows the translocation of bacteria (products) into the liver, aggravating inflammation and disease progression [1-3].

Our previous and current results point to a dual mechanism by which SIRT1 overexpression contributes to cholestasis disease progression; i) increased BA-mediated hepatocellular cell death [27], coupled with ii) increased inflammation mediated by the hyper-activation of macrophages overall aggravating cellular damage. The increased intestinal permeability observed in SIRT^{oe} mice could exacerbate macrophage activation and consequently hepatocellular liver damage. Our results in mice receiving SIRT^{oe} myeloid cells support the direct detrimental impact of these intrinsically hyper-activated proinflammatory macrophages in contributing to liver injury and cholestatic disease progression *in vivo*.

Our results pointing to a proinflammatory role of SIRT1 overexpression are in agreement with previous work in liver cancer where SIRT1 promoted proinflammatory cytokine expression in macrophages [51]. As well, the inhibition of Sirtuins reduced the production of proinflammatory cytokines in human macrophages from rheumatoid arthritis patients [52] and in immortalised macrophages in a NF- κ B dependent manner [53]. Interestingly, these observations are in contrast to the anti-inflammatory effects reported by Yeung et al, where the activation of SIRT1 by resveratrol inhibited NF- κ B activation *in vitro*

[31]. Similarly, Pfluger and colleagues showed that SIRT1 overexpressing mice had reduced inflammation when fed with a high fat diet [28].

To gain mechanistic insights into the proinflammatory function of SIRT1 we observed *in vivo* (Fig1, 2), we performed *in vitro* studies on BMDM where we found that the overexpression of SIRT1 associated with a delayed p65 activation after LPS rather than a complete inhibition as described by Yeung et al [31]. The different cell type used (non-small cancer cells) and the use of resveratrol, which can activate alternative pathways independently of SIRT1 [54] could explain the discrepancy with our results.

Macrophages sense dying cells and bacteria via PRRs (e.g. TLR) that activate the inflammasome leading to proinflammatory cytokine production [12]. The regulation of the inflammasome and the production of IL1 β we observed *in vivo* and *in vitro* could result from the activation of different pathways, including the stabilisation of Nlrp3 that can occur independently of NF- κ B-mediated *de novo* protein synthesis [55]. The activation of the inflammasome and IL1 β production can be also regulated by mTOR [8]; a key mediator of the activation of macrophages [8, 16, 20, 56]. Accordingly, our results showed increased activation of the mTORC1 pathway in SIRT1^{oe} BMDM in response to LPS that was supported by elevated pS6 and pULK⁷⁵⁷ expression. Moreover, our results showed that SIRT1 overexpressing macrophages were more dependent on mTOR to promote IL1 β production than WT cells in response to LPS. These results are interesting as the activation of SIRT1 with resveratrol has shown to inhibit the mTOR pathway [57], while others have described the synergy of SIRT1/mTORC1 activation in regulating cell response to stress [58]. Likewise, the inhibition of SIRT1 related to suppressed mTOR activation and resulted in reduced inflammation and damage in the lung after infection [59]. Notably, SIRT1 is necessary to activate mTOR downstream signalling via the deacetylation of S6 Kinase1, allowing its phosphorylation and activation of its kinase activity that phosphorylates ribosomal protein S6 [60]. This positive crosstalk was also described in human fibroblasts, where overexpression of SIRT1 correlated with increased S6K1 phosphorylation [61]. Most

prominently, the coordinated activation of SIRT1 and mTORC1 promotes intestinal stem cell expansion in response to calorie restriction, where deacetylation of S6K1 by SIRT1 enhances mTORC1 activation [58]. Overall, our results support that SIRT1 and mTORC1 can cooperate in cell stress conditions where cells require extensive energy like inflammation.

mTOR also regulates macrophage activation by inhibiting autophagy [20] via mechanisms involving the inhibition of ULK1 by phosphorylation of the Ser757 [11]. Autophagy is an essential mechanism to preserve cell metabolic and energy homeostasis as well as to control the host response to pathogens [11]. Thus, autophagy controls the activation of the inflammasome and IL1 β production by mediating the degradation of pro-IL1 β [10]. Likewise, impaired autophagy after loss of ATG16L1 enhanced the inflammasome activity and IL1 β production in macrophages after LPS [40] and during Chron's disease [62].

The attenuation of autophagy we observe when SIRT1 is overexpressed could result from mTORC1-mediated negative regulation of autophagy via increased and sustained phosphorylation of ULK⁷⁵⁷ as we observed in LPS-treated SIRT^{oe} BMDM. Alternatively, SIRT1 overexpression could regulate autophagy directly by contributing to the accumulation of p62, a negative regulator of autophagy [41]. Indeed, our finding is in accordance with a recent study showing that the overexpression of SIRT1 in liver tumoral cells contributes to the accumulation of p62 and activation of mTOR, thus inhibiting autophagy and contributing to tumor progression and poor prognosis in patients [63]. In turn, the stabilisation of p62 in the context of SIRT1 overexpression could contribute to increase mTORC1 signalling in SIRT^{oe} BMDM since p62 is essential to mediate the activation of the mTORC1 pathway via S6K1 activation [64].

During the last decade, there have been remarkable advances in our understanding of the influence of metabolism in controlling immune cell activation; the so-called immunometabolism. It is now known that during activation, macrophages undergo a metabolic rewiring analogous to the Warburg effect occurring in cancer cells [65], where

aerobic glycolysis supports macrophage effector function [7]. In addition to glycolysis, the activation of macrophages associates with the rewiring of the TCA cycle that leads to the accumulation of intermediates; citrate, succinate and fumarate [7], all with immunoregulatory functions. Citrate is key to produce itaconate, a potent antimicrobial [44, 66] by the downregulation of IDH [44, 46]. Itaconate also supports inflammation by inhibiting SDH and thus contributing to accumulation of succinate and sustained glycolytic reprogramming [43]. Succinate promotes glycolysis and proinflammatory cytokine production (IL1 β) in macrophages [9], providing an additional layer of interaction between cell metabolism and inflammation. Our results in BMDM confirmed that the overexpression of SIRT1, and concomitant activation of mTORC1, promotes the metabolic rewiring of macrophages, characterised by increased use of glucose carbons in a 'broken' TCA cycle and accumulation of immunomodulatory metabolites including citrate, succinate and malate. These findings along with our observations *in vivo*, where the adoptive transfer of SIRT1 overexpressing myeloid cells aggravates liver injury and fibrosis, support future studies where the modulation of SIRT1 could be used as a strategy to rewire macrophage metabolism and regulate inflammation. This strategy could as well reduce the inflammasome activation, which others and we have shown to contribute to liver injury and fibrosis during cholestatic disease [1, 2, 14, 15, 33]. In line with this, previous work showed the efficacy of the adoptive transfer of anti-inflammatory macrophage to effectively reduce liver fibrosis in mice [49] and more recently, macrophage therapy has been established as clinically safe supporting the use of these promising approaches to treat chronic liver disease [67].

Overall, our results provide novel mechanistic insights into the role of SIRT1 in regulating liver inflammation and warrant future research to define the potential of metabolic regulation of macrophages, via modulating SIRT1, as a therapeutic approach to treat cholestatic liver disease.

MATERIAL AND METHODS

Experimental procedures in animals

All experimental procedures were performed in 8–12-week-old male mice at the Disease Modelling Unit (University of East Anglia, UK). All experiments were approved by the Animal Welfare and Ethical Review Body (AWERB, University of East Anglia, Norwich, UK). All procedures were carried out following the guidelines of the National Academy of Sciences (National Institutes of Health, publication 86-23, revised 1985) and were performed within the provisions of the Animals (Scientific Procedures) Act 1986 (ASPA) and the LASA Guiding Principles for Preparing for Undertaking Aseptic Surgery (2010) under UK Home Office approval (70/8929).

SIRT1 overexpressing mice (SIRT^{oe}) were generated on a *C57/B6J* background as previously described [68]. Transplantation of isolated WT or SIRT^{oe} bone marrow cells into recipient PepCBoy mice was performed as previously described [69].

Cholestasis was induced by bile duct ligation (BDL) as described previously [27]. Septic liver injury was induced by intraperitoneal injection of lipopolysaccharide (LPS) (*Escherichia coli* E055:B5, Sigma) at a dose of 20mg/kg of body weight for up to 14 hours or by intraperitoneal administration of 35mg/kg LPS and 700mg/kg D-galactosamine (LPS/GalN) for up to 6 hours.

Determination of liver damage

Alanine aminotransferase (ALT) and aspartate aminotransferase (AST) were determined in mouse serum using the Randox Daytona analyser (Daytona) following the manufacturer's instructions as we previously described [27].

Isolation of primary hepatocytes

Primary hepatocytes were isolated as previously described [27]. Primary cells were exposed to 100ng/ml of LPS for 24 hours after which apoptotic cell death was determined by Caspase-3 activity assay as we described [27].

Bone marrow derived macrophage differentiation and culture

Bone marrow derived macrophages (BMDM) were differentiated from bone marrow cells isolated from WT and SIRT^{oe} mice. The femur and tibia were flushed with Roswell Park Memorial Institute (RPMI) media, bone marrow cells were pelleted and plated with RPMI medium containing 10% fetal bovine serum and 30% L929 conditioned media and differentiated for 7 days. Fresh media was added at day 3 after plating. 1×10^6 adherent cells were then plated for experiments in 6-well plates.

BMDM from WT and SIRT^{oe} animals were cultured in the presence of 100ng/ml LPS for up to 24 hours. For determination of autophagy, all cells were pre-treated with 20mM NH₄Cl and 100 μ M Leupeptin to inhibit lysosomal proteolysis, 2 hours before LPS treatment.

Histology, immunohistochemistry and immunofluorescence

Liver tissues were fixed in 10% neutral buffered formalin (Sigma). Liver tissues were embedded in paraffin and subsequent tissue blocks were sectioned, dewaxed and hydrated. For pathological analysis, liver sections were stained with Haematoxylin and Eosin (H&E) as we described previously [1, 27]. Immunohistochemistry (IHC) was carried out using an anti-CK19 antibody (Developmental Studies Hybridoma Bank, University of Iowa) as we described previously [1, 27]. Also, anti-CD11b (Abcam) and anti-F4/80 (Bio-Rad ABD serotec limited) were used as we previously described [70]. Quantification was carried out using Fiji software and is shown as the percentage of stained area relative to the total area per field. 5-10 fields per sample were imaged and analysed.

Fibrosis was determined using Sirius Red staining and immunofluorescence (IF) using a Cy3-conjugated α -smooth muscle actin antibody (Sigma). For IF, nuclei were counterstained with DAPI. The quantification of collagen fibres was performed using Fiji software and is represented as the percentage of stained area relative to total area per field. 5-10 fields per sample were imaged and analysed.

Immunofluorescence imaging of liver sections was performed using anti-Nlrp3 (Santa Cruz), anti-CD11b (Abcam) and anti-Ly6C (Myltenyi BioTec) primary antibodies followed by secondary Cy-3-anti-mouse (for Nlrp3) and FITC-anti-rabbit and FITC-anti-rat for CD11b and Ly6C respectively. Slides were counterstained and mounted with Vectashield Antifade mounting medium with DAPI (Vector).

For immunofluorescence imaging of BMDM, cells were grown on glass coverslips and were fixed with ice cold 30% acetone 70% methanol for 15 minutes at 4°C. Cells were washed and blocked with 10% goat serum, 0.01% Triton X-100, 1% BSA in PBS. Cells were incubated overnight with anti-p65 (Santa Cruz biotechnology) or LC3 (Cell Signaling Technology) in 1% BSA in PBS. Cells were washed and incubated for 1 hour with goat anti-rabbit Alexa Fluor 568 secondary (ThermoFisher Scientific) in 1% BSA in PBS. Cells were washed and mounted using Vectashield Antifade mounting medium with DAPI (Vector).

Metabolic determinations

Isolated and differentiated WT and SIRT^{oe} BMDM cell cultures were washed with 1XDPBS, followed by the addition of SILAC RPMI 1640 media (Gibco) supplemented with 11 mM of the 13C6 glucose tracer (Sigma), 2mM of 12C5 glutamine (ROTH) along with arginine and lysine, without FBS. Cells were starved for 4hours, following the addition of 100 ng/mL of LPS for 3 and 6hours.

After 3 and 6 hour LPS incubation, plates were washed once with 2mL of 0.9% NaCl (Sigma). Intracellular metabolites were extracted by adding 400 μ L of methanol (-20 °C) and 400 μ L ddH₂O (4 °C) containing 1 μ g/ml D6-glutaric acid (internal standard IS). Cells were scrapped and transferred to a tube containing 400 μ L chloroform (-20 °C) and mixed for 20 min at 1400 rpm and 4 °C (Eppendorf ThermoMixer C). Polar, aqueous, and non-polar phases were separated by centrifugation (5 min 21,000xg 4 °C) and 300 μ L of the polar phase were transferred to GC glass vial. Vials were vacuum-dried at 4 °C, capped and stored at -80 °C for further analysis.

Derivatization of samples was performed with an Axel Semrau Chronect Robotic Pal RTC directly before GC-MS measurement. 15 μ L of 2 % methoxyamine hydrochloride in pyridine was added to the samples following agitation for 60 min at 40 °C. Afterwards, an equal volume of N-Methyl-N-(trimethylsilyl)trifluoroacetamide was added and shaking continued for 30 min at the same temperature. 1 μ L of each derivatized sample was injected in splitless mode into a SSL injector heated to 270 °C. The gas chromatographic separation was performed on an Agilent 7890B GC equipped with a 30 m ZB-35 + 5 m duraguard column (Phenomenex). Helium was used as carrier gas with a flow rate of 1 mL/min. Initially, the GC oven temperature was held at 80 °C for 6 minutes. Afterwards, the temperature was raised by 6 °C/min until 300 °C were reached, and finally held for 10 min. Then, the temperature was increased to 325 °C at 10 °C/min and held for additional 4 minutes, resulting in a total run time of 59.167 min for one sample. The GC system was coupled to an Agilent 5977B MSD. Electrical ionization of the metabolites was performed at 70 eV. The MS ion source was constantly heated to 230 °C and the quadrupole to 150 °C. For the untargeted approach full scan mass spectra were acquired from m/z 70 to m/z 800. For the labeling experiments the connected detector was operating in selected ion monitoring. GC-MS chromatograms were processed using the inhouse developed software MetaboliteDetector, v3.320200313 [71]. Mass isotopomer distributions were calculated according to the chemical formulas from Wegner et al. [72].

RNA isolation and Quantitative Real-Time PCR

RNA was isolated from liver samples or cell cultures using QiAzol lysis Reagent (Qiagen). First strand synthesis and reverse transcription was performed using M-MLV Reverse Transcriptase (Invitrogen). Quantitative Real-Time PCR (qPCR) was carried out using SYBR Green reagent (Life Technologies) using the ViiA7 Real-time PCR detection system (Applied Biosystems). Gene expression was normalised to TATA-box binding protein 1 (TBP1) and is represented in times versus control sample gene expression. Primer sequences can be provided upon request.

Western blot analysis and ELISA

Proteins were extracted from snap frozen livers or cultured BMDM using RIPA buffer containing 50mM Tris-HCL, 150mM NaCl, 0.1% SDS, 2mM EDTA, 5% sodium deoxycholate, 1% Igepal 630, 1mM PMSF and protease inhibitor (Sigma).

Proteins were resolved using sodium dodecyl sulfate-polyacrylamide gels and transferred to nitrocellulose membranes (Whatman). Membranes were probed with interleukin 1 β , Caspase 1, Nlrp3, TLR2 and TLR4 (all from Santa Cruz Biotechnologies), as well as with Poly (ADP-ribose) polymerase (PARP), phospho-S6 ribosomal protein (pS6), p62, pULK⁷⁵⁷, Light Chain 3 A/B (LC3 A/B) (all from Cell Signaling Technologies). β -actin (Sigma Aldrich), GAPDH or α -Tubulin (Abcam) were used as loading controls. We used anti-rabbit IgG-HRP-linked or anti-mouse IgG-HRP linked secondary antibodies (Cell Signaling Technologies).

Expression of IL1 β was determined in BMDM protein extracts while IL-10 and IL-4 were determined in whole liver protein extracts using R&D systems DuoSet according to the manufacturer's instructions.

Flow Cytometry

Immune cells were isolated from mouse liver as we described previously[1, 27]. Immune cells were stained with CD45-APC-Cy7 (BD), CD11b-PE (BD), F4/80-FITC (Myltenyi), and Ly6C-Pacific blue (MACS). Flow cytometry was carried out using BD LSR-Fortessa.

Analysis was performed using FlowJo software.

Statistical analysis

Data are expressed as mean \pm standard error of the mean. Statistical significance was determined using two-way analysis of variance (ANOVA) followed by Student's t test or Student's t test only, as appropriate, using GraphPad Prism software.

REFERENCES

- [1] Isaacs-Ten A, Echeandia M, Moreno-Gonzalez M, Brion A, Goldson A, Philo M, Patterson AM, Parker A, Galduroz M, Baker D, Rushbrook SM, Hildebrand F, Beraza N. Intestinal Microbiome-Macrophage Crosstalk Contributes to Cholestatic Liver Disease by Promoting Intestinal Permeability in Mice. *Hepatology* 2020;72(6):2090-108.
- [2] Liao L, Schneider KM, Galvez EJC, Frissen M, Marschall HU, Su H, Hatting M, Wahlstrom A, Haybaeck J, Puchas P, Mohs A, Peng J, Bergheim I, Nier A, Hennings J, Reissing J, Zimmermann HW, Longerich T, Strowig T, Liedtke C, Cubero FJ, Trautwein C. Intestinal dysbiosis augments liver disease progression via NLRP3 in a murine model of primary sclerosing cholangitis. *Gut* 2019;68(8):1477-92.
- [3] Tripathi A, Debelius J, Brenner DA, Karin M, Loomba R, Schnabl B, Knight R. The gut-liver axis and the intersection with the microbiome. *Nat Rev Gastroenterol Hepatol* 2018;15(7):397-411.
- [4] Karlmark KR, Weiskirchen R, Zimmermann HW, Gassler N, Ginhoux F, Weber C, Merad M, Luedde T, Trautwein C, Tacke F. Hepatic recruitment of the inflammatory Gr1+ monocyte subset upon liver injury promotes hepatic fibrosis. *Hepatology* 2009;50(1):261-74.
- [5] Guicciardi ME, Trussoni CE, Krishnan A, Bronk SF, Lorenzo Pisarello MJ, O'Hara SP, Splinter PL, Gao Y, Vig P, Revzin A, LaRusso NF, Gores GJ. Macrophages contribute to the pathogenesis of sclerosing cholangitis in mice. *J Hepatol* 2018;69(3):676-86.
- [6] Pradere JP, Kluwe J, De Minicis S, Jiao JJ, Gwak GY, Dapito DH, Jang MK, Guenther ND, Mederacke I, Friedman R, Dragomir AC, Aloman C, Schwabe RF. Hepatic macrophages but not dendritic cells contribute to liver fibrosis by promoting the survival of activated hepatic stellate cells in mice. *Hepatology* 2013;58(4):1461-73.
- [7] Ryan DG, O'Neill LAJ. Krebs cycle rewired for macrophage and dendritic cell effector functions. *FEBS Lett* 2017;591(19):2992-3006.
- [8] Moon JS, Hisata S, Park MA, DeNicola GM, Ryter SW, Nakahira K, Choi AMK. mTORC1-Induced HK1-Dependent Glycolysis Regulates NLRP3 Inflammasome Activation. *Cell Rep* 2015;12(1):102-15.
- [9] Tannahill GM, Curtis AM, Adamik J, Palsson-McDermott EM, McGettrick AF, Goel G, Frezza C, Bernard NJ, Kelly B, Foley NH, Zheng L, Gardet A, Tong Z, Jany SS, Corr SC, Haneklaus M, Caffrey BE, Pierce K, Walmsley S, Beasley FC, Cummins E, Nizet V, Whyte M, Taylor CT, Lin H, Masters SL, Gottlieb E, Kelly VP, Clish C, Auron PE, Xavier RJ, O'Neill LA. Succinate is an inflammatory signal that induces IL-1beta through HIF-1alpha. *Nature* 2013;496(7444):238-42.
- [10] Harris J, Hartman M, Roche C, Zeng SG, O'Shea A, Sharp FA, Lambe EM, Creagh EM, Golenbock DT, Tschopp J, Kornfeld H, Fitzgerald KA, Lavelle EC. Autophagy controls IL-1beta secretion by targeting pro-IL-1beta for degradation. *J Biol Chem* 2011;286(11):9587-97.
- [11] Ma Y, Galluzzi L, Zitvogel L, Kroemer G. Autophagy and cellular immune responses. *Immunity* 2013;39(2):211-27.
- [12] Lamkanfi M, Dixit VM. Mechanisms and functions of inflammasomes. *Cell* 2014;157(5):1013-22.
- [13] Cai SY, Ge M, Mennone A, Hoque R, Ouyang X, Boyer JL. Inflammasome Is Activated in the Liver of Cholestatic Patients and Aggravates Hepatic Injury in Bile Duct-Ligated Mouse. *Cell Mol Gastroenterol Hepatol* 2020;9(4):679-88.

- [14] Frissen M, Liao L, Schneider KM, Djudjaj S, Haybaeck J, Wree A, Rolle-Kampczyk U, von Bergen M, Latz E, Boor P, Trautwein C. Bidirectional Role of NLRP3 During Acute and Chronic Cholestatic Liver Injury. *Hepatology* 2021;73(5):1836-54.
- [15] Inzaugarat ME, Johnson CD, Holtmann TM, McGeough MD, Trautwein C, Papouchado BG, Schwabe R, Hoffman HM, Wree A, Feldstein AE. NLR Family Pyrin Domain-Containing 3 Inflammasome Activation in Hepatic Stellate Cells Induces Liver Fibrosis in Mice. *Hepatology* 2019;69(2):845-59.
- [16] Byles V, Covarrubias AJ, Ben-Sahra I, Lamming DW, Sabatini DM, Manning BD, Horng T. The TSC-mTOR pathway regulates macrophage polarization. *Nat Commun* 2013;4:2834.
- [17] Cheng SC, Quintin J, Cramer RA, Shepardson KM, Saeed S, Kumar V, Giamarellos-Bourboulis EJ, Martens JH, Rao NA, Aghajani-refah A, Manjeri GR, Li Y, Ifrim DC, Arts RJ, van der Veer BM, Deen PM, Logie C, O'Neill LA, Willems P, van de Veerdonk FL, van der Meer JW, Ng A, Joosten LA, Wijmenga C, Stunnenberg HG, Xavier RJ, Netea MG. mTOR- and HIF-1 α -mediated aerobic glycolysis as metabolic basis for trained immunity. *Science* 2014;345(6204):1250684.
- [18] Albert V, Hall MN. mTOR signaling in cellular and organismal energetics. *Curr Opin Cell Biol* 2015;33:55-66.
- [19] Laplante M, Sabatini DM. mTOR signaling in growth control and disease. *Cell* 2012;149(2):274-93.
- [20] Ko JH, Yoon SO, Lee HJ, Oh JY. Rapamycin regulates macrophage activation by inhibiting NLRP3 inflammasome-p38 MAPK-NF κ B pathways in autophagy- and p62-dependent manners. *Oncotarget* 2017;8(25):40817-31.
- [21] Houtkooper RH, Pirinen E, Auwerx J. Sirtuins as regulators of metabolism and healthspan. *Nat Rev Mol Cell Biol* 2012;13(4):225-38.
- [22] Lin SJ, Defossez PA, Guarente L. Requirement of NAD and SIR2 for life-span extension by calorie restriction in *Saccharomyces cerevisiae*. *Science* 2000;289(5487):2126-8.
- [23] Guarente L. Calorie restriction and sirtuins revisited. *Genes Dev* 2013;27(19):2072-85.
- [24] Garcia-Rodriguez JL, Barbier-Torres L, Fernandez-Alvarez S, Gutierrez-de Juan V, Monte MJ, Halilbasic E, Herranz D, Alvarez L, Aspichueta P, Marin JJ, Trauner M, Mato JM, Serrano M, Beraza N, Martinez-Chantar ML. SIRT1 controls liver regeneration by regulating bile acid metabolism through farnesoid X receptor and mammalian target of rapamycin signaling. *Hepatology* 2014;59(5):1972-83.
- [25] Fang Y, Nicholl MB. Sirtuin 1 in malignant transformation: friend or foe? *Cancer Lett* 2011;306(1):10-4.
- [26] Chen HC, Jeng YM, Yuan RH, Hsu HC, Chen YL. SIRT1 promotes tumorigenesis and resistance to chemotherapy in hepatocellular carcinoma and its expression predicts poor prognosis. *Ann Surg Oncol* 2012;19(6):2011-9.
- [27] Blokker BA, Maijo M, Echeandia M, Galduroz M, Patterson AM, Ten A, Philo M, Schungel R, Gutierrez-de Juan V, Halilbasic E, Fuchs C, Le Gall G, Milkiewicz M, Milkiewicz P, Banales JM, Rushbrook SM, Mato JM, Trauner M, Muller M, Martinez-Chantar ML, Varela-Rey M, Beraza N. Fine-Tuning of Sirtuin 1 Expression Is Essential to Protect the Liver From Cholestatic Liver Disease. *Hepatology* 2019;69(2):699-716.
- [28] Pfluger PT, Herranz D, Velasco-Miguel S, Serrano M, Tschop MH. Sirt1 protects against high-fat diet-induced metabolic damage. *Proc Natl Acad Sci U S A* 2008;105(28):9793-8.

- [29] Schug TT, Xu Q, Gao H, Peres-da-Silva A, Draper DW, Fessler MB, Purushotham A, Li X. Myeloid deletion of SIRT1 induces inflammatory signaling in response to environmental stress. *Mol Cell Biol* 2010;30(19):4712-21.
- [30] Yang H, Zhang W, Pan H, Feldser HG, Lainez E, Miller C, Leung S, Zhong Z, Zhao H, Sweitzer S, Considine T, Riera T, Suri V, White B, Ellis JL, Vlasuk GP, Loh C. SIRT1 activators suppress inflammatory responses through promotion of p65 deacetylation and inhibition of NF-kappaB activity. *PLoS One* 2012;7(9):e46364.
- [31] Yeung F, Hoberg JE, Ramsey CS, Keller MD, Jones DR, Frye RA, Mayo MW. Modulation of NF-kappaB-dependent transcription and cell survival by the SIRT1 deacetylase. *EMBO J* 2004;23(12):2369-80.
- [32] Yoshizaki T, Schenk S, Imamura T, Babendure JL, Sonoda N, Bae EJ, Oh DY, Lu M, Milne JC, Westphal C, Bandyopadhyay G, Olefsky JM. SIRT1 inhibits inflammatory pathways in macrophages and modulates insulin sensitivity. *Am J Physiol Endocrinol Metab* 2010;298(3):E419-28.
- [33] Hou L, Yang L, Chang N, Zhao X, Zhou X, Dong C, Liu F, Yang L, Li L. Macrophage Sphingosine 1-Phosphate Receptor 2 Blockade Attenuates Liver Inflammation and Fibrogenesis Triggered by NLRP3 Inflammasome. *Front Immunol* 2020;11:1149.
- [34] Tacke F, Zimmermann HW. Macrophage heterogeneity in liver injury and fibrosis. *J Hepatol* 2014;60(5):1090-6.
- [35] Orecchioni M, Ghosheh Y, Pramod AB, Ley K. Macrophage Polarization: Different Gene Signatures in M1(LPS+) vs. Classically and M2(LPS-) vs. Alternatively Activated Macrophages. *Front Immunol* 2019;10:1084.
- [36] Ramachandran P, Pellicoro A, Vernon MA, Boulter L, Aucott RL, Ali A, Hartland SN, Snowdon VK, Cappon A, Gordon-Walker TT, Williams MJ, Dunbar DR, Manning JR, van Rooijen N, Fallowfield JA, Forbes SJ, Iredale JP. Differential Ly-6C expression identifies the recruited macrophage phenotype, which orchestrates the regression of murine liver fibrosis. *Proc Natl Acad Sci U S A* 2012;109(46):E3186-95.
- [37] Giordano DM, Pinto C, Maroni L, Benedetti A, Marzioni M. Inflammation and the Gut-Liver Axis in the Pathophysiology of Cholangiopathies. *Int J Mol Sci* 2018;19(10).
- [38] Cabrera-Rubio R, Patterson AM, Cotter PD, Beraza N. Cholestasis induced by bile duct ligation promotes changes in the intestinal microbiome in mice. *Sci Rep* 2019;9(1):12324.
- [39] Triger DR, Boyer TD, Levin J. Portal and systemic bacteraemia and endotoxaemia in liver disease. *Gut* 1978;19(10):935-9.
- [40] Saitoh T, Fujita N, Jang MH, Uematsu S, Yang BG, Satoh T, Omori H, Noda T, Yamamoto N, Komatsu M, Tanaka K, Kawai T, Tsujimura T, Takeuchi O, Yoshimori T, Akira S. Loss of the autophagy protein Atg16L1 enhances endotoxin-induced IL-1beta production. *Nature* 2008;456(7219):264-8.
- [41] Katsuragi Y, Ichimura Y, Komatsu M. p62/SQSTM1 functions as a signaling hub and an autophagy adaptor. *FEBS J* 2015;282(24):4672-8.
- [42] O'Neill LA. A broken krebs cycle in macrophages. *Immunity* 2015;42(3):393-4.
- [43] Lampropoulou V, Sergushichev A, Bambouskova M, Nair S, Vincent EE, Loginicheva E, Cervantes-Barragan L, Ma X, Huang SC, Griss T, Weinheimer CJ, Khader S, Randolph GJ, Pearce EJ, Jones RG, Diwan A, Diamond MS, Artyomov MN. Itaconate Links Inhibition of Succinate Dehydrogenase with Macrophage Metabolic Remodeling and Regulation of Inflammation. *Cell Metab* 2016;24(1):158-66.

- [44] Michelucci A, Cordes T, Ghelfi J, Pailot A, Reiling N, Goldmann O, Binz T, Wegner A, Tallam A, Rausell A, Buttini M, Linster CL, Medina E, Balling R, Hiller K. Immune-responsive gene 1 protein links metabolism to immunity by catalyzing itaconic acid production. *Proc Natl Acad Sci U S A* 2013;110(19):7820-5.
- [45] Cordes T, Wallace M, Michelucci A, Divakaruni AS, Sapcariu SC, Sousa C, Koseki H, Cabrales P, Murphy AN, Hiller K, Metallo CM. Immunoresponsive Gene 1 and Itaconate Inhibit Succinate Dehydrogenase to Modulate Intracellular Succinate Levels. *J Biol Chem* 2016;291(27):14274-84.
- [46] Meiser J, Kramer L, Sapcariu SC, Battello N, Ghelfi J, D'Herouel AF, Skupin A, Hiller K. Pro-inflammatory Macrophages Sustain Pyruvate Oxidation through Pyruvate Dehydrogenase for the Synthesis of Itaconate and to Enable Cytokine Expression. *J Biol Chem* 2016;291(8):3932-46.
- [47] Weindl D, Cordes T, Battello N, Sapcariu SC, Dong X, Wegner A, Hiller K. Bridging the gap between non-targeted stable isotope labeling and metabolic flux analysis. *Cancer Metab* 2016;4:10.
- [48] Duffield JS, Forbes SJ, Constandinou CM, Clay S, Partolina M, Vuthoori S, Wu S, Lang R, Iredale JP. Selective depletion of macrophages reveals distinct, opposing roles during liver injury and repair. *J Clin Invest* 2005;115(1):56-65.
- [49] Thomas JA, Pope C, Wojtacha D, Robson AJ, Gordon-Walker TT, Hartland S, Ramachandran P, Van Deemter M, Hume DA, Iredale JP, Forbes SJ. Macrophage therapy for murine liver fibrosis recruits host effector cells improving fibrosis, regeneration, and function. *Hepatology* 2011;53(6):2003-15.
- [50] Hirschfield GM, Heathcote EJ, Gershwin ME. Pathogenesis of cholestatic liver disease and therapeutic approaches. *Gastroenterology* 2010;139(5):1481-96.
- [51] Zhou B, Yang Y, Li C. SIRT1 inhibits hepatocellular carcinoma metastasis by promoting M1 macrophage polarization via NF-kappaB pathway. *Onco Targets Ther* 2019;12:2519-29.
- [52] Grabiec AM, Krausz S, de Jager W, Burakowski T, Groot D, Sanders ME, Prakken BJ, Maslinski W, Eldering E, Tak PP, Reedquist KA. Histone deacetylase inhibitors suppress inflammatory activation of rheumatoid arthritis patient synovial macrophages and tissue. *J Immunol* 2010;184(5):2718-28.
- [53] Fernandes CA, Fievez L, Neyrinck AM, Delzenne NM, Bureau F, Vanbever R. Sirtuin inhibition attenuates the production of inflammatory cytokines in lipopolysaccharide-stimulated macrophages. *Biochem Biophys Res Commun* 2012;420(4):857-61.
- [54] Baur JA, Ungvari Z, Minor RK, Le Couteur DG, de Cabo R. Are sirtuins viable targets for improving healthspan and lifespan? *Nat Rev Drug Discov* 2012;11(6):443-61.
- [55] Guo H, Callaway JB, Ting JP. Inflammasomes: mechanism of action, role in disease, and therapeutics. *Nat Med* 2015;21(7):677-87.
- [56] Li K, Zhang Y, Liang KY, Xu S, Zhou XJ, Tan K, Lin J, Bai XC, Yang CL. Rheb1 deletion in myeloid cells aggravates OVA-induced allergic inflammation in mice. *Sci Rep* 2017;7:42655.
- [57] Ghosh HS, McBurney M, Robbins PD. SIRT1 negatively regulates the mammalian target of rapamycin. *PLoS One* 2010;5(2):e9199.
- [58] Igarashi M, Guarente L. mTORC1 and SIRT1 Cooperate to Foster Expansion of Gut Adult Stem Cells during Calorie Restriction. *Cell* 2016;166(2):436-50.
- [59] Huang J, Tian R, Yang Y, Jiang R, Dai J, Tang L, Zhang L. The SIRT1 inhibitor EX-527 suppresses mTOR activation and alleviates acute lung injury in mice with endotoxemia. *Innate Immun* 2017;23(8):678-86.

- [60] Hong S, Zhao B, Lombard DB, Fingar DC, Inoki K. Cross-talk between sirtuin and mammalian target of rapamycin complex 1 (mTORC1) signaling in the regulation of S6 kinase 1 (S6K1) phosphorylation. *J Biol Chem* 2014;289(19):13132-41.
- [61] Huang J, Gan Q, Han L, Li J, Zhang H, Sun Y, Zhang Z, Tong T. SIRT1 overexpression antagonizes cellular senescence with activated ERK/S6k1 signaling in human diploid fibroblasts. *PLoS One* 2008;3(3):e1710.
- [62] Plantinga TS, Crisan TO, Oosting M, van de Veerdonk FL, de Jong DJ, Philpott DJ, van der Meer JW, Girardin SE, Joosten LA, Netea MG. Crohn's disease-associated ATG16L1 polymorphism modulates pro-inflammatory cytokine responses selectively upon activation of NOD2. *Gut* 2011;60(9):1229-35.
- [63] Feng L, Chen M, Li Y, Li M, Hu S, Zhou B, Zhu L, Yu L, Zhou Q, Tan L, An H, Wang X, Jin H. Sirt1 deacetylates and stabilizes p62 to promote hepatocarcinogenesis. *Cell Death Dis* 2021;12(4):405.
- [64] Duran A, Amanchy R, Linares JF, Joshi J, Abu-Baker S, Porollo A, Hansen M, Moscat J, Diaz-Meco MT. p62 is a key regulator of nutrient sensing in the mTORC1 pathway. *Mol Cell* 2011;44(1):134-46.
- [65] Warburg O. On the origin of cancer cells. *Science* 1956;123(3191):309-14.
- [66] Jha AK, Huang SC, Sergushichev A, Lampropoulou V, Ivanova Y, Loginicheva E, Chmielewski K, Stewart KM, Ashall J, Everts B, Pearce EJ, Driggers EM, Artyomov MN. Network integration of parallel metabolic and transcriptional data reveals metabolic modules that regulate macrophage polarization. *Immunity* 2015;42(3):419-30.
- [67] Moroni F, Dwyer BJ, Graham C, Pass C, Bailey L, Ritchie L, Mitchell D, Glover A, Laurie A, Doig S, Hargreaves E, Fraser AR, Turner ML, Campbell JDM, McGowan NWA, Barry J, Moore JK, Hayes PC, Leeming DJ, Nielsen MJ, Musa K, Fallowfield JA, Forbes SJ. Safety profile of autologous macrophage therapy for liver cirrhosis. *Nat Med* 2019;25(10):1560-5.
- [68] Herranz D, Munoz-Martin M, Canamero M, Mulero F, Martinez-Pastor B, Fernandez-Capetillo O, Serrano M. Sirt1 improves healthy ageing and protects from metabolic syndrome-associated cancer. *Nat Commun* 2010;1:3.
- [69] Mistry JJ, Marlein CR, Moore JA, Hellmich C, Wojtowicz EE, Smith JGW, Macaulay I, Sun Y, Morfakis A, Patterson A, Horton RH, Divekar D, Morris CJ, Haestier A, Di Palma F, Beraza N, Bowles KM, Rushworth SA. ROS-mediated PI3K activation drives mitochondrial transfer from stromal cells to hematopoietic stem cells in response to infection. *Proc Natl Acad Sci U S A* 2019;116(49):24610-9.
- [70] Fernandez-Alvarez S, Gutierrez-de Juan V, Zubiete-Franco I, Barbier-Torres L, Lahoz A, Pares A, Luka Z, Wagner C, Lu SC, Mato JM, Martinez-Chantar ML, Beraza N. TRAIL-producing NK cells contribute to liver injury and related fibrogenesis in the context of GNMT deficiency. *Lab Invest* 2015;95(2):223-36.
- [71] Hiller K, Hangebrauk J, Jäger C, Spura J, Schreiber K, Schomburg D. MetaboliteDetector: comprehensive analysis tool for targeted and nontargeted GC/MS based metabolome analysis. *Anal Chem* 2009;81(9):3429-39.
- [72] Wegner A, Weindl D, Jäger C, Sapcariu SC, Dong X, Stephanopoulos G, Hiller K. Fragment Formula Calculator (FFC): Determination of Chemical Formulas for Fragment Ions in Mass Spectrometric Data. *Anal Chem* 2014;86(4):2221-8.

FIGURE LEGENDS

Figure 1. The overexpression of SIRT1 promotes inflammation in mice after bile duct ligation. (A) Cell sorting strategy to isolate CD11b⁺/F4/80⁺ macrophages from livers from WT mice before and 7 days after BDL. **(B)** qPCR analysis on isolated macrophages from livers showing increased SIRT1 expression after BDL in WT mice. **(C)** qPCR analysis showing increased SIRT1 expression in macrophages isolated from SIRT^{oe} mice compared to WTs. **(D)** IHC using an anti-F4/80 and **(E)** anti-CD11b Ab in paraffin-embedded liver sections and further quantification showing increased presence of macrophages in SIRT^{oe} mice compared to WTs after BDL. **(F)** Gating strategy to detect increased presence of infiltrating macrophages in livers from SIRT^{oe} mice compared to WTs 7 days after BDL by FACS. **(G)** Quantification after FACS analysis of immune cells isolated from livers showing increased infiltration of macrophages 7 days after BDL. n=4-9 animals/treatment group were analysed; Values are mean ± SEM. **P* < 0.05, ***P* < 0.01 (WT vs SIRT^{oe}). Representative microscopical images are shown at 10x (D, E).

Figure 2. The overexpression of SIRT1 associates with increased Nlrp3-inflammasome activation in CD11b⁺ cells and Ly6C⁺ macrophages in the liver in response to BDL. (A) qPCR analysis of liver extracts supporting increased expression of pathogen receptors (TLR) and inflammasome components **(B)** Western blot analysis confirming increased TLRs, Nlrp3, cleaved Caspase1 and IL1β supporting activation of the inflammasome in SIRT^{oe} livers after BDL. **(C)** Immunofluorescence showing colocalization of Nlrp3 (Red) and CD11b (Green) and **(D)** Nlrp3 (Red) and Ly6C (Green) and **(E)** IL1β (Red) and Ly6C (Green) in liver sections 7days after BDL. Cell nuclei are in blue stained with DAPI. **(F)** qPCR analysis showing increased IL1β expression in macrophages isolated from SIRT^{oe} mice compared to WTs. **(G)** ELISA on whole liver protein extracts showing increased expression of IL-10 and **(H)** IL-4 in SIRT^{oe} livers compared to WTs at 7 days after BDL and control mice. **(I)** Quantification of circulating FITC in serum samples from WT and SIRT^{oe}

mice 3 and 7 days after BDL supporting increased intestinal permeability in SIRT^{oe} animals. n=4-9 animals/treatment group were analysed; Values are mean \pm SEM. * P < 0.05, ** P < 0.01 (WT vs SIRT^{oe}). Representative microscopical images are shown at 20x (C-E) magnification.

Figure 3. The overexpression of SIRT1 promotes increased liver injury and

inflammasome activation in response to endotoxin. (A) Quantification of liver injury blood markers (ALT and AST) indicates increased liver injury in SIRT^{oe} mice 6 hours after LPS/GalN treatment. **(B)** H&E staining of liver sections from WT and SIRT^{oe} mice confirms more severe parenchymal damage in LPS/GalN-SIRT^{oe} mice. **(C)** Western blot analysis supported increased apoptosis in LPS/GalN-SIRT^{oe} mice compared to LPS/GalN-WTs. **(D)** IHC in paraffin-embedded liver sections using an anti-F4/80 and **(E)** anti-CD11b Ab, followed by quantification show increased presence of macrophages in livers from SIRT^{oe} mice compared to WTs 6 hours after LPS/GalN. n=5-6 animals/treatment group were analysed; Values are mean \pm SEM. * P < 0.05, ** P < 0.01 (WT vs SIRT^{oe}). Representative microscopical images are shown at 4x (B), 10x (D, E).

Figure 4. The overexpression of SIRT1 promotes inflammasome activation in

response to endotoxin. (A) qPCR analysis of liver extracts indicates increased expression of TLR and inflammasome components. **(B)** Western blot analysis showing higher expression of cleaved IL1 β supporting activation of the inflammasome in SIRT^{oe} livers 6 hours after LPS/GalN. **(C)** Immunofluorescence showing colocalization of Nlrp3 (Red) and CD11b (Green) and **(D)** Nlrp3 (Red) and Ly6C (Green) and **(E)** IL1 β (Red) and Ly6C (Green) in liver sections from WT and SIRT^{oe} mice 6 hours after LPS/GalN. **(F)** Primary hepatocytes and BMDM from WT mice were exposed to 100ng/ml of LPS and IL1 β , **(G)** Caspase1 and **(H)** Nlrp3 gene expression was analysed by qPCR showing increased response in BMDM compared to hepatocytes which show only a marginal response.

Slides were mounted on a solution containing DAPI (blue) staining cell nuclei. n=5-6 animals/treatment group were analysed; Values are mean \pm SEM. $**P < 0.01$, $***P < 0.001$ (WT vs SIRT^{oe}). Representative microscopical images are shown at 20x (C-E) magnification. Results from in vitro experiments are representative analysis of n=3 replicates per timepoint, per cell type. Values are mean \pm SEM. $*P < 0.05$, $**P < 0.01$ (WT vs SIRT^{oe}).

Figure 5. The overexpression of SIRT1 promotes increased liver injury and

inflammasome activation in response to LPS. (A) Quantification of liver injury markers

(ALT and AST) in serum samples indicates increased liver injury in SIRT^{oe} mice 14 hours

after LPS treatment. **(B)** qPCR analysis and **(C)** Western blot analysis shows increased

IL1 β gene expression and cleavage, overall supporting the activation of the inflammasome in

SIRT^{oe} livers 6 hours after LPS. **(D)** Caspase3 activity was quantified showing mild impact of

LPS in WT hepatocyte cell death that was not increased in SIRT^{oe} primary hepatocytes.

n=4-7 animals/treatment group were analysed; Values are mean \pm SEM. $*P < 0.05$, $**P < 0.01$

(WT vs SIRT^{oe}). Results from in vitro experiments are representative analysis of n=3

replicates per timepoint.

Figure 6. The overexpression of SIRT1 promotes proinflammatory phenotype in bone marrow derived macrophages associated with activation of mTOR signalling and decreased autophagy. (A) Increased IL1 β secretion detected by ELISA on supernatants of

BMDM treated with 100ng/ml LPS for 24 hours **(B)** Immunocytochemistry on cultured BMDM

using an anti-p65 antibody (Red) indicates attenuated and delayed translocation of p65 into

the nucleus in SIRT^{oe} BMDM after LPS. Experiments were done twice in triplicate. Values

are mean \pm SEM. $*P < 0.05$, $**P < 0.01$, $***P < 0.001$ (WT vs SIRT^{oe}). Representative

microscopical images are shown at 20x magnification.

Figure 7. The overexpression of SIRT1 promotes activation of mTOR signalling and decreased autophagy in bone marrow derived macrophages. (A) Western blot analysis shows earlier and increased phosphorylation of S6 in SIRT^{oe} BMDM after LPS. **(B)** ELISA of BMDM supernatants that were pretreated with 50nM of Rapamycin 1 hour before LPS treatment for 24 hours showed stronger decrease in IL1 β secretion in SIRT^{oe} BMDM compared to WT cells (expressed in % of reduction). **(C)** Western blot analysis showing increased phosphorylation of ULK in serine 757 and increased accumulation of p62 in SIRT^{oe} BMDM in response to LPS compared to WT cells. To evaluate autophagy, lysosomal proteolysis was inhibited by pretreating cells with 20mM NH₄Cl and 100 μ M Leupeptin at 2 hours before LPS treatment. In these conditions, **(D)** western blot analysis shows increased accumulation of lipidated LC3II in LPS/WT BMDM compared to LPS/ SIRT^{oe} cells that shows lower LC3II but higher LC3I expression. **(E)** Attenuated autophagy in LPS/ SIRT^{oe} BMDM was confirmed by ICC using anti-LC3 antibody (green). **(F)** Further quantification shows decreased presence of fluorescent-labeled LC3 compared to the WTs, which show increased LC3 staining 2 and 3 hours after LPS. Experiments were done twice in triplicate. Values are mean \pm SEM. * P < 0.05, ** P < 0.01 (WT vs SIRT^{oe}). Representative microscopical images are shown at 20x magnification.

Figure 8. Metabolome analysis of WT and SIRT^{oe} BMDMs. (A) Analysis of intracellular metabolite abundances. Signal intensities (peak area) were normalized to an internal standard D6-glutaric acid. **(B)** Scheme of atom transitions in the TCA cycle using a [U-¹³C]-glucose tracer. ¹²C-carbons are illustrated in light grey and ¹³C-carbons in dark grey. PDH, pyruvate dehydrogenase; CSY, citrate synthase; IRG1, aconitate decarboxylase; ACO, aconitase; IDH, isocitrate dehydrogenase; AKGDH, α -ketoglutarate dehydrogenase; SDH, succinate dehydrogenase; FH, fumarate hydratase; MDH, malate dehydrogenase. **(C)** MID of citrate as well as the relative abundances of M1-itaconate and M2-succinate and -malate. **(D)** Ratio of M4/M2-isotopologues of succinate and malate, indicating TCA cycling rate.

Error bars indicate standard error. Statistical significance was determined via Student's t-test (*, $p < 0.05$; **, $p < 0.01$; ***, $p < 0.001$; ns, not significant; Ctrl $n=3$, SIRT^{oe} $n=2$).

Figure 9. Adoptive transfer of SIRT^{oe} bone marrow cells contributes to cholestatic disease progression after BDL. (A) Western blot analysis showing that BM-derived cells from SIRT^{oe} have increased SIRT1 expression when compared to cells obtained from WT mice. **(B)** FACS analysis of BM cells isolated from WT (CD45.2) showing cell engraftment in recipient PEPC mice (CD45.1) **(C)** Serum levels of liver injury markers and **(D)** H&E staining of liver sections from PEPCBoy mice receiving bone marrow cells from WT or SIRT^{oe} mice analysed at 7 days after BDL show increased liver injury in SIRT^{oe}/PEPCmice. **(E)** Western blot analysis of whole liver lysates showing increased Caspase-1 cleavage and **(F)** IL1 β cleaved protein expression in SIRT^{oe}/PEPCmice 7 days after BDL. **(G)** IHC using an anti-CK19 Ab in paraffin-embedded liver sections showing enhanced ductular reaction in SIRT^{oe}/PEPCmice compared to WT/PEPCmice. **(H)** Liver fibrosis was assessed by Sirius Red staining and **(I)** α SMA immunofluorescence on liver sections from transplanted mice 7 days after BDL. Images at 4x (D) and 10x (G-I) are representative of $n=4-5$ animals/treatment group; Values are mean \pm SEM. * $P < 0.05$, ** $P < 0.01$, *** $P < 0.001$ [GF vs GF+WT]).

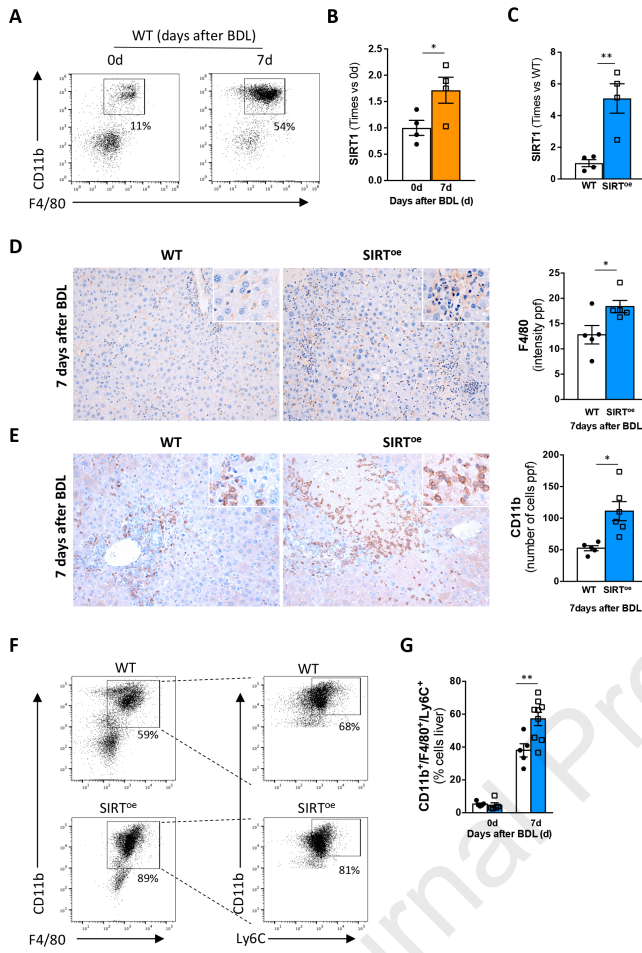


Figure 1

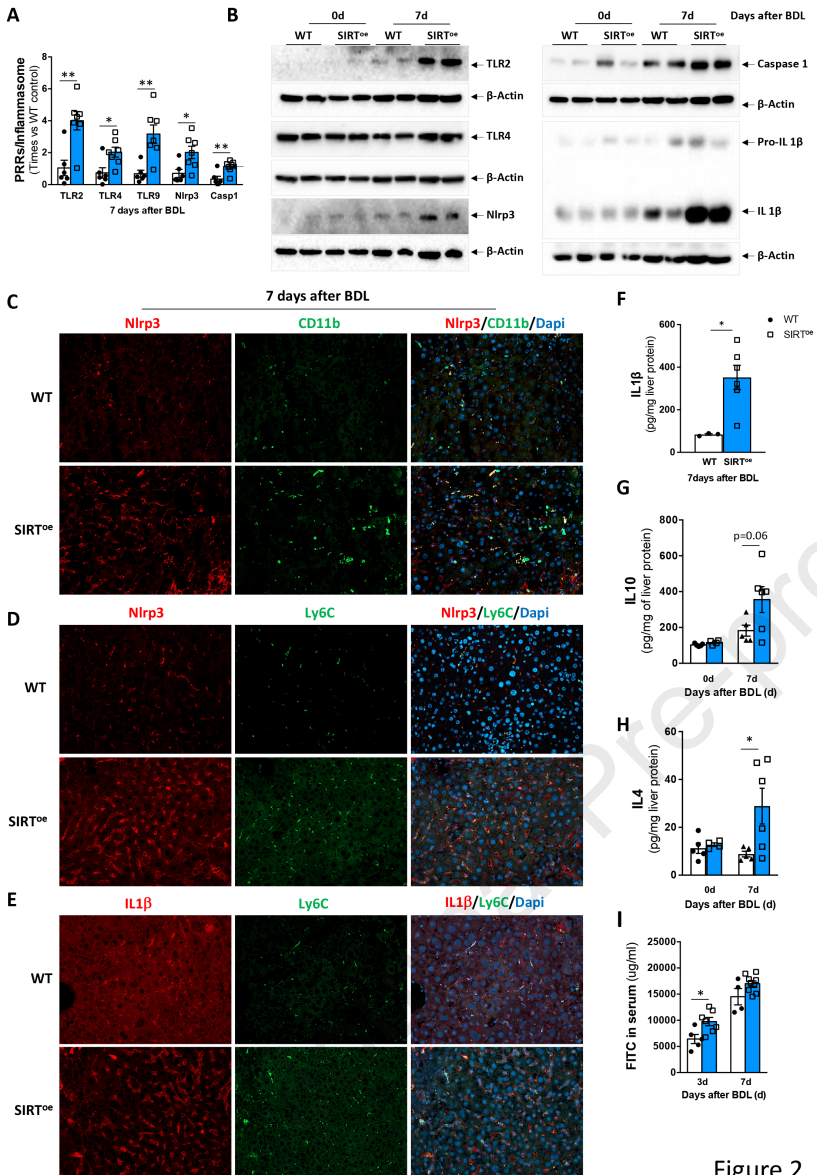


Figure 2

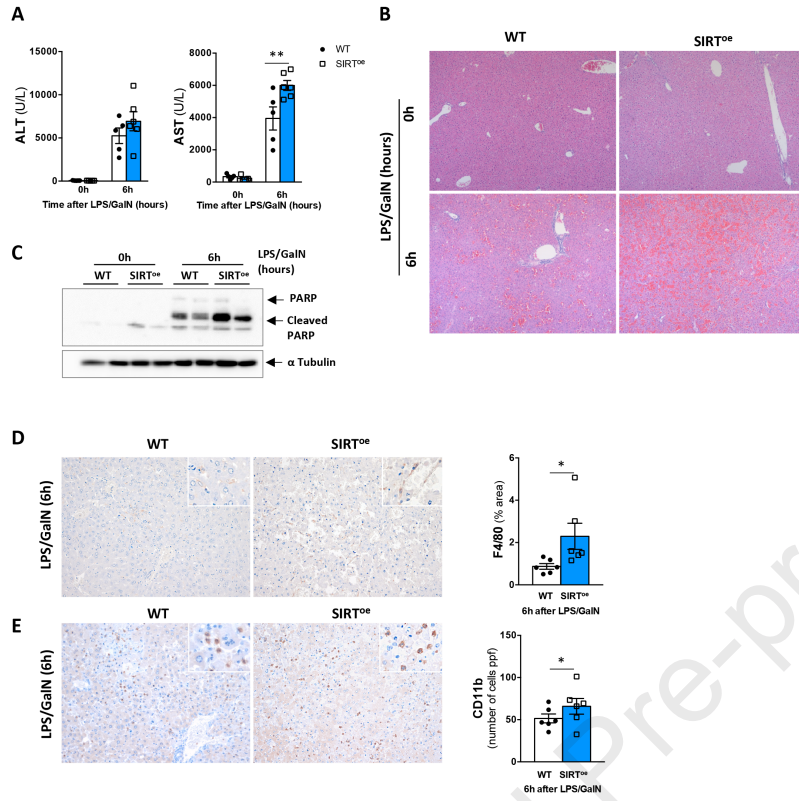


Figure 3

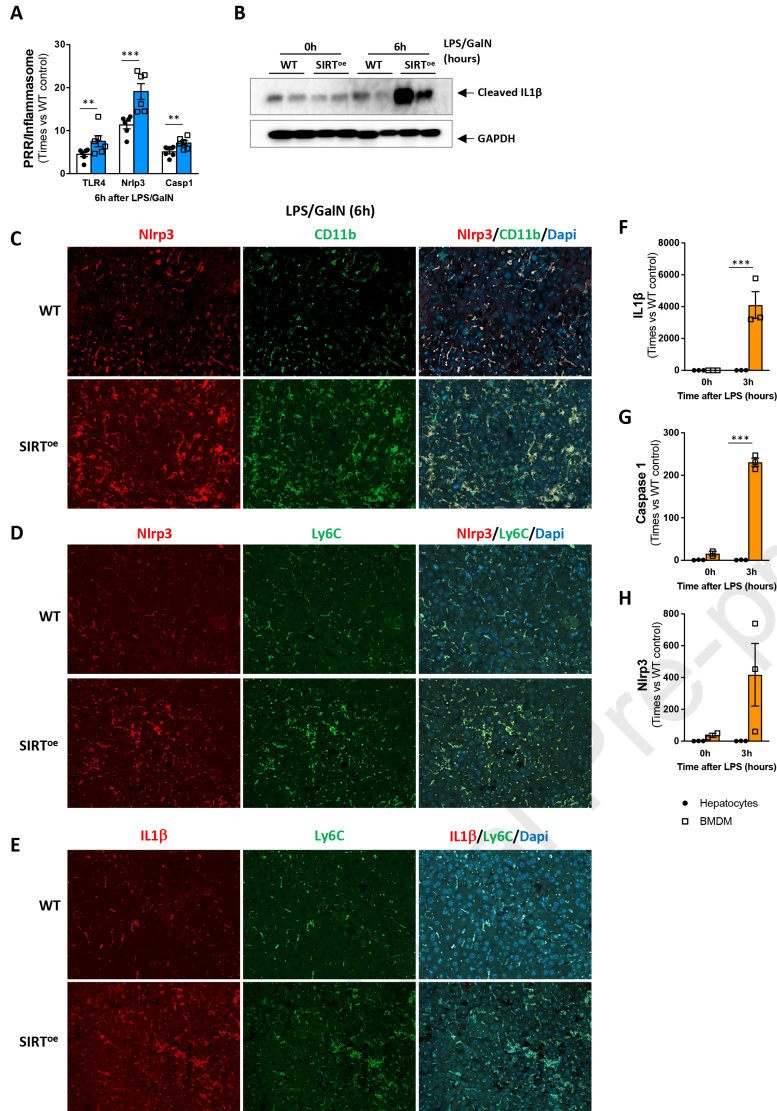


Figure 4

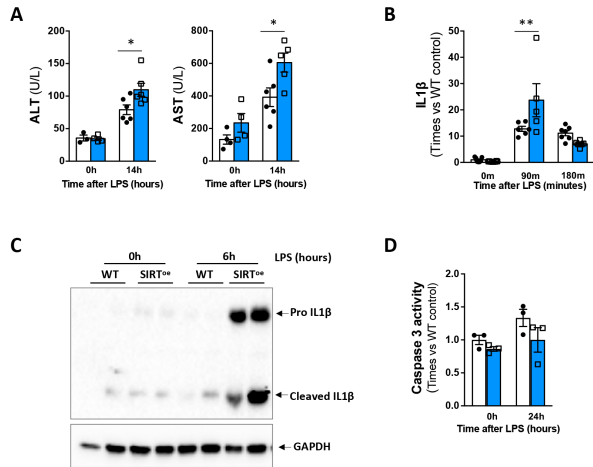


Figure 5

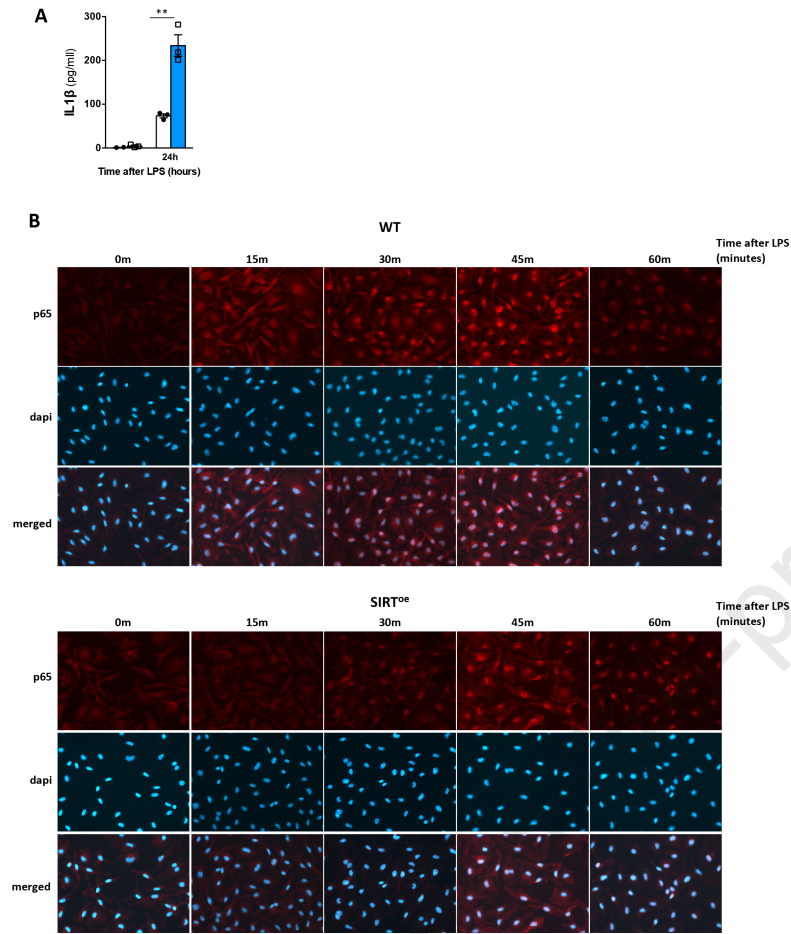


Figure 6

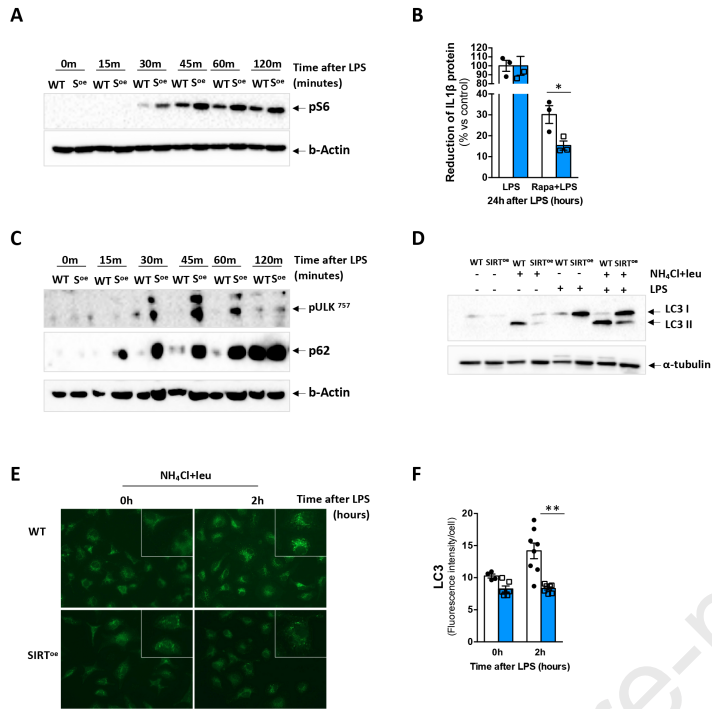


Figure 7

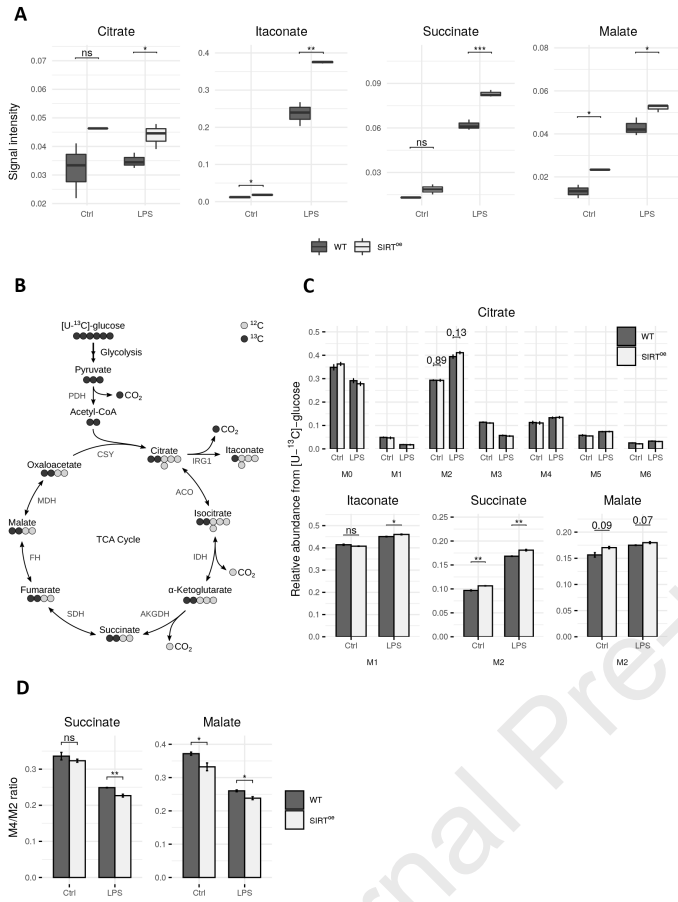


Figure 8

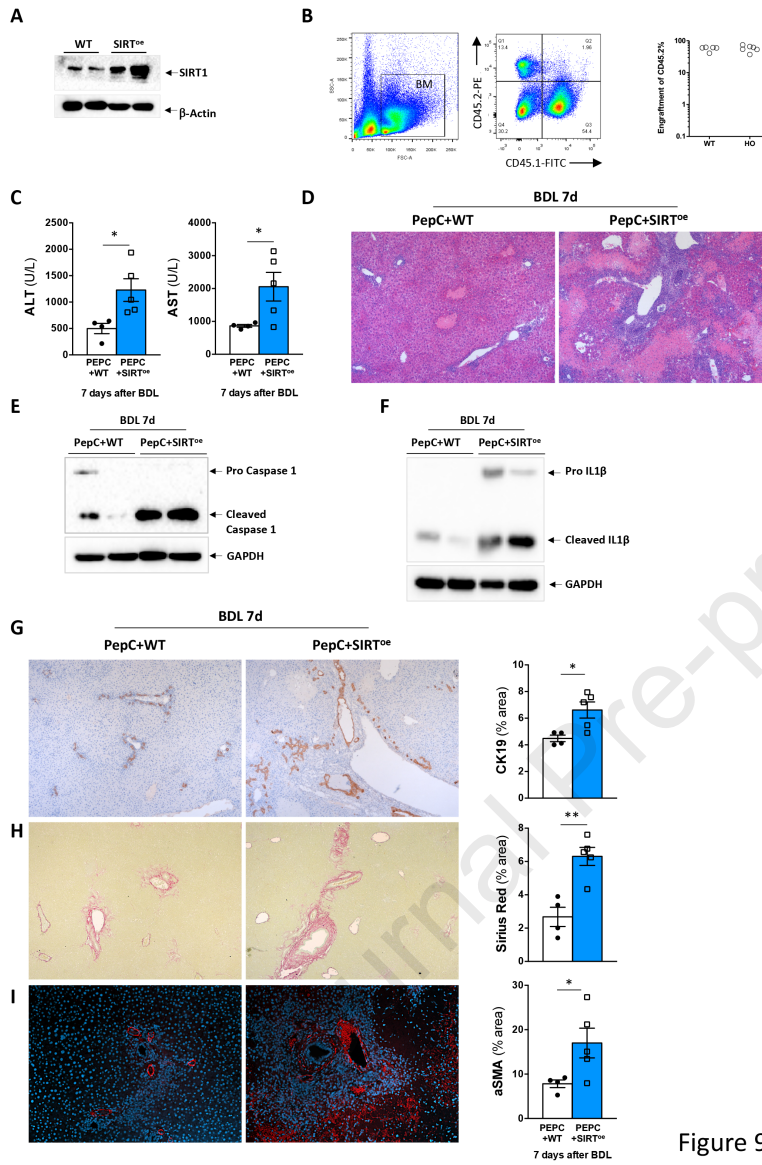


Figure 9